

# Atmospheric Pressure Chemical Vapor Deposition: An Alternative Route to Large-Scale MoS<sub>2</sub> and WS<sub>2</sub> Inorganic Fullerene-like Nanostructures and Nanoflowers\*\*

Xiao-Lin Li, Jian-Ping Ge, and Ya-Dong Li\*[a]

**Abstract:** Large-scale MoS<sub>2</sub> and WS<sub>2</sub> inorganic fullerene-like (IF) nanostructures (onionlike nanoparticles, nanotubes) and elegant three-dimensional nanoflowers (NF) have been selectively prepared through an atmospheric pressure chemical vapor deposition (APCVD) process with the reaction of chlorides and sulfur. The morphologies

were controlled by adjusting the deposition position, the deposition temperature, and the flux of the carrier gas. All of the nanostructures have been char-

**Keywords:** chemical vapor deposition • nanoflowers • nanostructures • sulfides

acterized by X-ray powder diffraction (XRD), transmission electron microscopy (TEM), and scanning electron microscopy (SEM). A reaction mechanism is proposed based on the experimental results. The surface area of MoS<sub>2</sub> IF nanoparticles and the field-emission effect of as-prepared WS<sub>2</sub> nanoflowers is reported.

## Introduction

Fullerene structures of carbon were first discovered in the 1980s,<sup>[1-2]</sup> and extensive investigations of their many applications in batteries, optics, and electronics was carried out soon after the large-scale synthesis methods were reported.<sup>[3]</sup> Molybdenum disulfide (MoS<sub>2</sub>), tungsten disulfide (WS<sub>2</sub>), and many other layered inorganic compounds were found to have a comparable structure to carbon and could form inorganic fullerene-like (IF) structures under appropriate conditions.<sup>[4-11]</sup> Much effort has been devoted to the synthesis of these novel IF materials. MoS<sub>2</sub> and WS<sub>2</sub> are versatile transition-metal sulfides and have attracted much attention due to their distinctive properties and wide ranges of promising applications, such as solid lubricants,<sup>[12]</sup> solid-state secondary lithium battery cathodes,<sup>[13]</sup> and industrial catalysts for hydro-desulfurization of crude oil.<sup>[14]</sup> Recently, the excellent performances of MoS<sub>2</sub> and WS<sub>2</sub> nanotubes in hydrogen storage, host-guest compounds, and scanning tunnelling microscope (STM) tips have been reported.<sup>[15-17]</sup>

The synthesis of MoS<sub>2</sub> and WS<sub>2</sub> IF nanostructures by various routes has been reported,<sup>[18-23]</sup> such as the gas-phase reaction between oxides and H<sub>2</sub>S/H<sub>2</sub>,<sup>[18-19]</sup> the decomposition of ammonium thiomolybdate or metal trisulfides,<sup>[20-21]</sup> the heating of MoS<sub>2</sub> powders,<sup>[22]</sup> and the catalyzed transport method.<sup>[23]</sup> Recently, we have synthesized WS<sub>2</sub> nanotubes from artificial lamellar structures.<sup>[24]</sup>

Despite the research being carried out globally on MoS<sub>2</sub> and WS<sub>2</sub> IF nanostructures, it will be several years before the commercial applications of these fullerene-based products, in areas such as catalysts, batteries, and lubricants, are realized. To enable scientists to extensively investigate the properties and applications of these nanostructures, a conventional and effective method for the large-scale synthesis of high-quality IF MoS<sub>2</sub> and WS<sub>2</sub> is a prerequisite. Tenne and co-workers met the challenge and obtained macroscopic quantities of WS<sub>2</sub> hollow onions by means of the fluidized-bed reactor.<sup>[25]</sup> Recently, we reported the simple reaction of MoO<sub>3</sub> nanobelts and S to synthesize IF MoS<sub>2</sub>.<sup>[26]</sup> Herein we describe a novel atmospheric pressure chemical vapor deposition (APCVD) route for the large-scale synthesis of MoS<sub>2</sub> and WS<sub>2</sub> IF nanostructures. These structures and elegant three-dimensional nanoflowers (NF) were obtained by the reaction of chlorides (MoCl<sub>5</sub>/WCl<sub>6</sub>) and sulfur, under controlled conditions; a reaction mechanism for the synthesis of these structures is proposed, and their surface area and field-emission properties measured. The APCVD strategy provides an alternative method for the large-scale synthesis of IF MoS<sub>2</sub> and WS<sub>2</sub> and might offer better opportunities for the further investigation of their properties and applications. It has also been explored

[a] X.-L. Li, J.-P. Ge, Prof. Y.-D. Li

Department of Chemistry and the Key Laboratory of Atomic & Molecular Nanosciences, Tsinghua University National Center for Nanoscience and Nanotechnology Beijing 100084 (P. R. China)  
Fax: (+86)106-278-8765  
E-mail: ydli@tsinghua.edu.cn

\*\*] Xiao-Lin Li and Jian-Ping Ge contributed equally to this work.

Supporting information for this article is available on the WWW under <http://www.chemeurj.org/> or from the author.

as a general approach for the synthesis of other metal sulfides.

## Results and Discussion

**MoS<sub>2</sub> and WS<sub>2</sub> fullerene-like nanoparticles:** X-ray diffraction (XRD) was used to determine the chemical composition and crystallinity of the products. Figure 1 shows the typical XRD patterns of IF MoS<sub>2</sub> and WS<sub>2</sub>. All the reflections in Figure 1a have been indexed to the hexagonal structure of MoS<sub>2</sub> with lattice constants:  $a=3.160$ ,  $c=12.29$  Å (JCPDS card No: 77-1716); and those of Figure 1b have been indexed to the hexagonal phase of WS<sub>2</sub> with lattice constants:  $a=3.153$ ,  $c=12.32$  Å (JCPDS card No: 84-1398). The (002) peaks in the images display a prominent signal indicating the presence of a well-stacked layered structure. A shift in the (002) peak position of IF MoS<sub>2</sub> and WS<sub>2</sub>, which is usually regarded as a key mechanism for the strain relief of the folded structure, was also observed in our investigation. From Figure 1a and b, it was estimated that the (002) peaks of IF MoS<sub>2</sub> and WS<sub>2</sub> were shifted by about 0.7 and 0.8%, values that are smaller than the corresponding value (about 2%) reported by Tenne et al.<sup>[4,18-19]</sup>

The size and morphology of the products were examined by transmission electron microscopy (TEM). Figure 2 shows the TEM images obtained for IF MoS<sub>2</sub> nanoparticles. On the basis of TEM, more than 95% of the samples were fullerene-like nanoparticles. Figure 2a–d are the representative

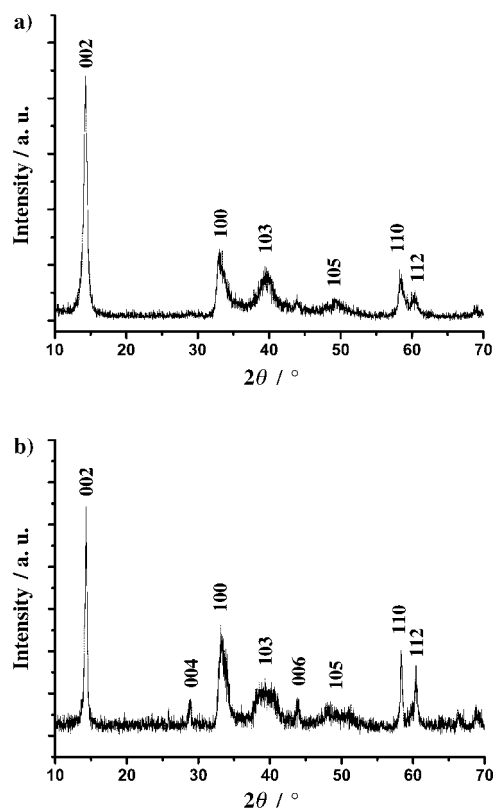


Figure 1. Typical XRD patterns of a) as-synthesized IF MoS<sub>2</sub> and b) IF WS<sub>2</sub>.

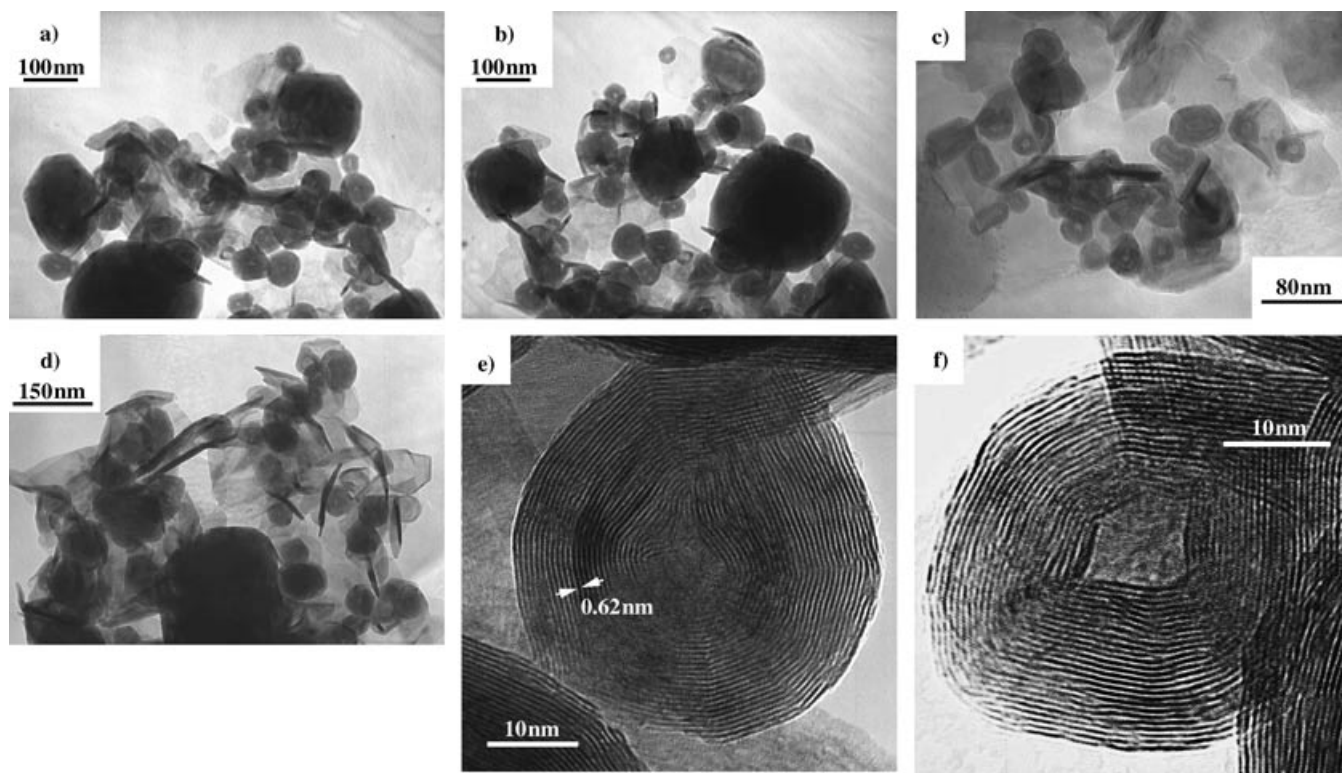


Figure 2. TEM images of MoS<sub>2</sub> IF nanoparticles show the hollow, spherical, and polyhedral morphologies (a–d). HRTEM images of individual MoS<sub>2</sub> fullerene-like nanoparticles show the lattice structure (e, f). The lattice fringe thickness is shown.

low-magnification TEM images, in which IF MoS<sub>2</sub> has a hollow spherical morphology with diameters of about 40 nm. High-resolution TEM (HRTEM) provided further insight into the structure of the individual IF MoS<sub>2</sub> nanoparticles. Figure 2e and f show the typical lattice structure. The distance between two lattice fringes was 0.62 nm. Some IF MoS<sub>2</sub> nanoparticles were polyhedral in shape, as seen in Figure 3, in which it is shown that by varying the tilt-angle

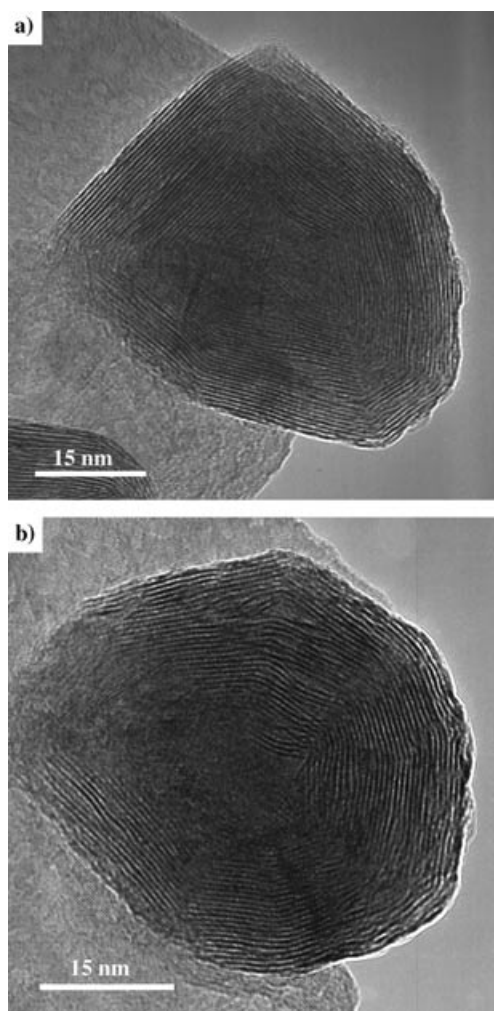


Figure 3. TEM images of an MoS<sub>2</sub> polyhedron observed at a tilt-angle of a) 0°, and b) 30°.

of the sample in the TEM, parts of the polyhedron fringe pattern disappear and a different fringe pattern appears on the other side of the nanostructure. This behavior means that either the structure is not completely closed or, as in the case of SnS<sub>2</sub>,<sup>[11]</sup> that the closed polyhedra are highly faceted. In addition, the shape of the MoS<sub>2</sub> polyhedron was very irregular, as is easily verified by looking at the tilted sample.

The low-magnification image in Figure 4a shows that the as-synthesized IF WS<sub>2</sub> particles are irregular in shape with diameters of about 50 nm. The HRTEM image of an indi-

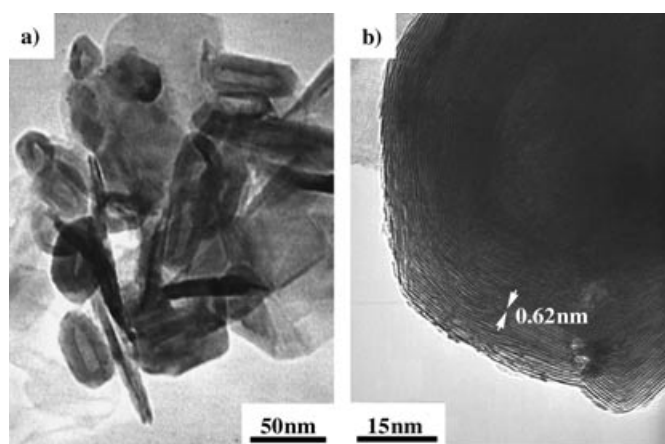


Figure 4. a) A typical TEM image of WS<sub>2</sub> fullerene-like nanoparticles. b) A HRTEM pattern of an individual IF WS<sub>2</sub> particle. The lattice fringe thickness is shown.

vidual WS<sub>2</sub> IF nanoparticle is shown in Figure 4b, from which the lattice fringes were measured to be about 0.62 nm thick.

Further observations showed that some IF MoS<sub>2</sub> and WS<sub>2</sub> nanoparticles contained many edge dislocations; consequently the layers were not fully closed, although they were curved. The inner hollow core of some nanoparticles exhibited distinct angles, some typically 90°, and some nanoparticles formed octahedra. The many defects and large diameters of the IF nanoparticles were believed to have relieved some strain in the folded layers and hence the (002) peak did not shift as much as the value reported by Tenne et al.<sup>[4,18–19]</sup>

Energy-dispersive spectroscopy (EDS) analysis was carried out on individual IF MoS<sub>2</sub> and WS<sub>2</sub> nanoparticles. The results confirmed that the molar ratio of sulfur to the corresponding metal was close to 2:1 (the spectra are not shown here).

**MoS<sub>2</sub> and WS<sub>2</sub> nanotubes and nanoflowers:** By adjusting reaction variables such as the deposition position, the deposition temperature, and the flux of the carrier gas, we obtained products with different morphologies. The temperature of the deposition positions had the most important influence on the product morphologies. We investigated the products deposited at temperatures from 400 to 850 °C. The results showed that MoS<sub>2</sub> and WS<sub>2</sub> onionlike nanoparticles were obtained in the chlorides' boat at about 850 °C. MoS<sub>2</sub> and WS<sub>2</sub> nanotubes were obtained at a deposition temperature of about 750 °C, whereas MoS<sub>2</sub> and WS<sub>2</sub> nanoflowers had the optimal morphology when deposited at about 650 °C.

Figure 5 presents the typical scanning electron microscopy (SEM) images of MoS<sub>2</sub> nanoflowers and nanotubes. Based on SEM, more than 95% of samples obtained at the deposition temperatures of 650 and 750 °C were nanoflowers and nanotubes, respectively. As shown in Figure 5a, MoS<sub>2</sub> nanoflowers are three-dimensional, partly spherical, and flower-like in appearance, several micrometers in size and composed of tens to hundreds of self-assembled petals. The

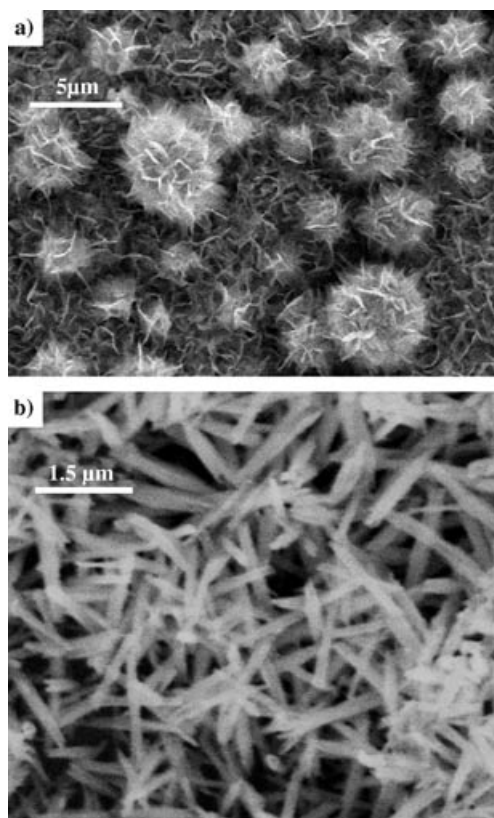


Figure 5. SEM images of MoS<sub>2</sub> a) nanoflowers and b) nanotubes.

petals emanate from one center and grow in all directions. They slightly curve and gradually attenuate towards the edges, resulting in 100–200 nm pieces with thin edges of about 10 nm (Figure 6a). Figure 5b shows a large amount of MoS<sub>2</sub> nanotubes. The nanotubes have a regular column shape and are several micrometers long. Some open-ended nanotubes can be seen in this image.

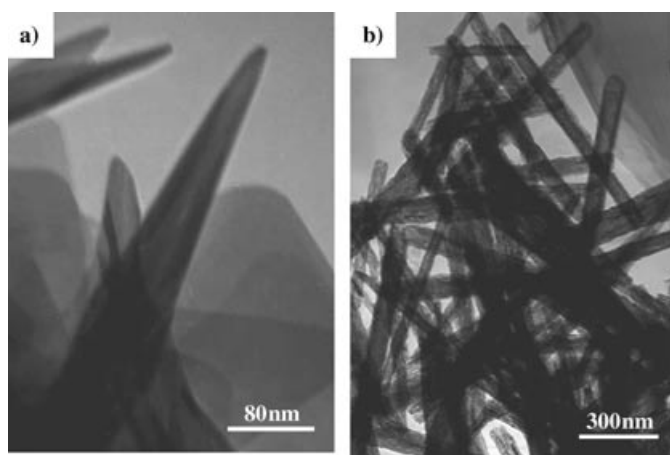


Figure 6. TEM images of MoS<sub>2</sub> a) nanoflowers and b) nanotubes.

TEM images of MoS<sub>2</sub> nanoflowers and nanotubes are shown in Figure 6. Petals of MoS<sub>2</sub> nanoflowers having large widths and thin edges can be seen in Figure 6a, which agrees

with the SEM results. MoS<sub>2</sub> nanotubes about a micrometer in length and having diameters ranging from 30 to 100 nm are shown in Figure 6b.

Nanoflowers and nanotubes of WS<sub>2</sub> were also examined by SEM and TEM measurements. Figure 7 shows the representative SEM results. Figure 7a is a low-magnification image of a large area of WS<sub>2</sub> nanoflowers. A more detailed image of an individual nanoflower is shown in Figure 7b; here tens to hundreds of petals, several micrometers in size, can be seen assembled into the flowerlike morphology. The WS<sub>2</sub> nanoflower petals are approximately 100–300 nm wide and 40 nm thick. Figure 7c shows large-scale WS<sub>2</sub> nanotubes several micrometers in length. A higher magnification SEM image (Figure 7d) shows that the diameter of the open-ended tube is about 40 nm. TEM images of WS<sub>2</sub> nanoflowers and nanotubes are shown in Figure 8. Here it is shown that the WS<sub>2</sub> nanoflower is composed of wide petals with thin curving edges (Figure 8a), in agreement with the SEM results. Figure 8b and c show the typical hollow structure of WS<sub>2</sub> nanotubes with diameters ranging from 20 to 50 nm. The inset of Figure 8b is the SAED (SAED = selected area electron diffraction) pattern taken on an individual WS<sub>2</sub> nanotube. The HRTEM image (figure 8d) shows that the as-synthesized nanotubes have thin and well-stacked walls with lattice fringes of about 0.62 nm.

#### Raman study of MoS<sub>2</sub> IF nanoparticles and nanoflowers:

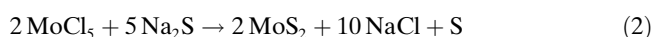
Taking MoS<sub>2</sub> as the example, we carried out a Raman study of the IF nanostructure and flowerlike (FL) samples. Figure 9a shows typical Raman spectra of MoS<sub>2</sub> fullerene-like nanoparticles and nanoflowers taken at room temperature. These Raman patterns are enlarged at different wavenumbers in Figure 9b–d. IF MoS<sub>2</sub> and FL samples appeared to have an analogous outline, however, further observation showed that their Raman spectra were quite different, both in peak shape and position. The frequencies of the peaks shown in Figure 9 are listed in Table 1 and correspond well to the symmetry modes reported in the literature.<sup>[27]</sup>

The Raman study of the IF structure and FL samples indicated that the particle size, crystal structure, and synthesis-specific structural modifications in these nanoparticles had brought about great changes in the electronic states.

**Reaction mechanism:** Reported strategies for the synthesis of sulfides,<sup>[8,26,28–30]</sup> especially the reactions between chlorides and a mixed gas of H<sub>2</sub>S and H<sub>2</sub>,<sup>[8,28]</sup> gives us a good understanding of the reaction mechanism of MoCl<sub>5</sub>/WCl<sub>6</sub> and S. In the well-known reaction of MoCl<sub>5</sub> and H<sub>2</sub>S/H<sub>2</sub>, H<sub>2</sub> is used as the additional reductant [Eq. (1)].<sup>[28]</sup>



Very recently, it was reported that the reaction of MoCl<sub>5</sub> (WCl<sub>6</sub>) and Na<sub>2</sub>S could self-ignite or be detonated with a hot filament at 40–60 °C.<sup>[30]</sup> In that reaction system, given in Equations (2) and (3), Na<sub>2</sub>S served as the reductant and sulfurization agent instead of H<sub>2</sub>S and H<sub>2</sub>.



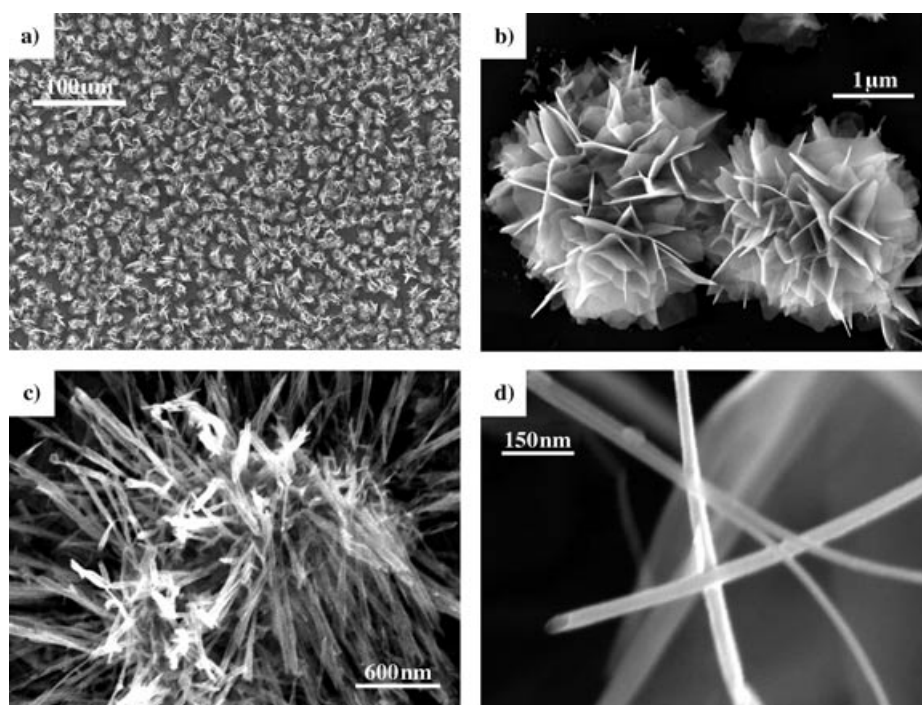


Figure 7. a) Low-magnification and b) high-magnification SEM images of WS<sub>2</sub> nanoflowers. c, d) SEM images of WS<sub>2</sub> nanotubes.

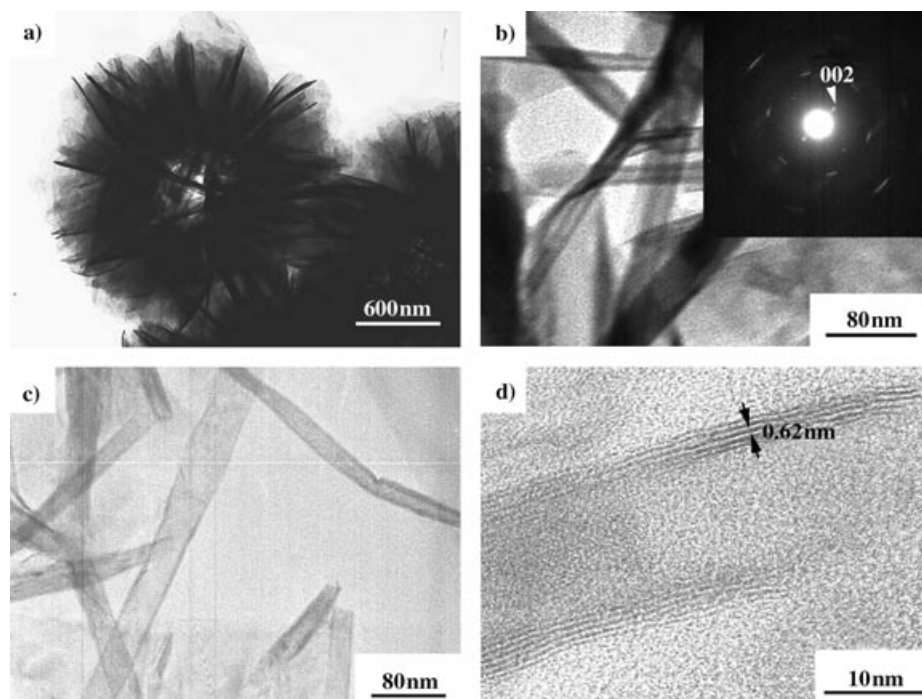


Figure 8. a) TEM images of WS<sub>2</sub> nanoflowers and b, c) nanotubes. The SAED pattern of an individual nanotube is shown in the inset of (b). d) A HRTEM image of a WS<sub>2</sub> nanotube showing its lattice fringes to be about 0.62 nm.



In our strategy, we used sulfur instead of Na<sub>2</sub>S or H<sub>2</sub>S/H<sub>2</sub> to react with the chlorides. At elevated temperatures, sulfur is reactive and might serve as the reductant and sulfurization agent at the same time.<sup>[26]</sup> The reaction of MoCl<sub>5</sub>/WCl<sub>6</sub> and S is a mixed process of self-redox and metathesis reac-

tions. Based on the experimental facts, the reactions between the chlorides and S were formulated as given in Equations (4) and (5).



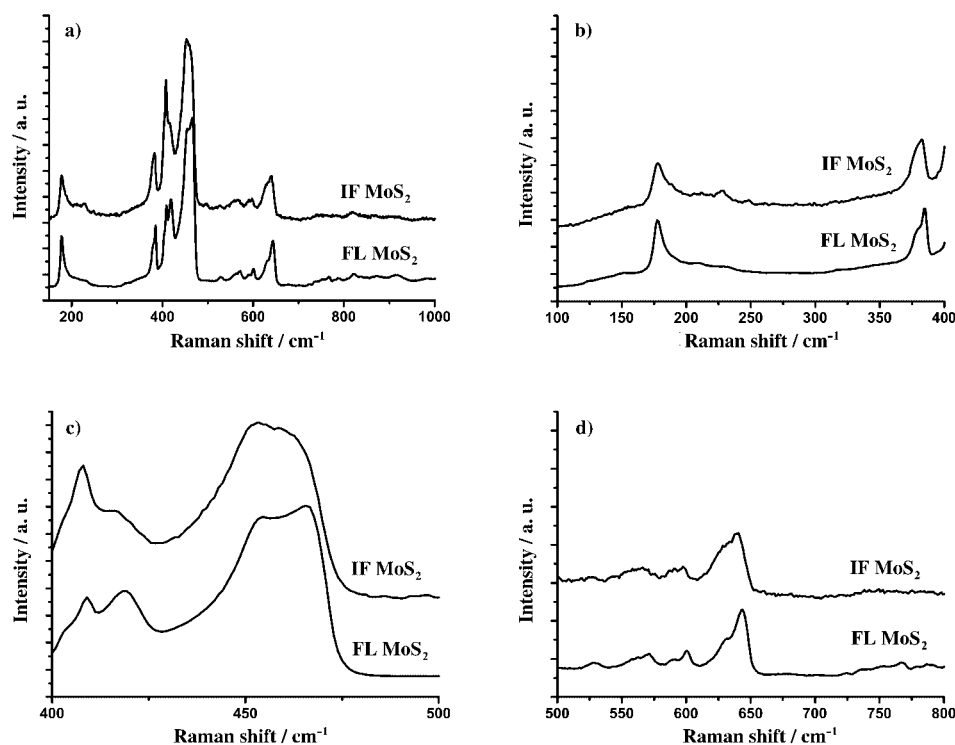


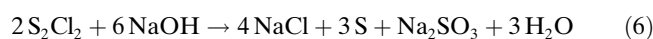
Figure 9. Raman spectra of IF MoS<sub>2</sub> and nanoflowers. a) The full spectra between wavenumbers 150 to 1000 cm<sup>-1</sup>; spectra enlarged at the corresponding wavenumbers of: b) 100 to 400 cm<sup>-1</sup>, c) 400 to 500 cm<sup>-1</sup>, and d) 500 to 800 cm<sup>-1</sup>.

Table 1. Raman peaks observed in IF and FL MoS<sub>2</sub> samples at room temperature and the corresponding symmetry assignments. All peak positions are in cm<sup>-1</sup>.

IF MoS <sub>2</sub>	FL MoS <sub>2</sub>	Symmetry assignment <sup>[a]</sup>
178	177	A <sub>1g</sub> (M)–LA(M)
228		LA(M)
383	385	E <sub>1g</sub> (Γ)
408	409	A <sub>1g</sub> (Γ)
416	419	
453	455	
460	466	2 × LA(M)
	529	E <sub>1g</sub> (M) + LA(M)
566	571	2 × E <sub>1g</sub> (Γ)
598	600	E <sub>1g</sub> (M) + LA(M)
640	643	A <sub>1g</sub> (M) + LA(M)

[a] LA refers to longitudinal acoustic, Γ and M refer to Γ and M points in the electronic-band structure diagrams.

The reaction was environmentally benign, because sulfur was used rather than hazardous H<sub>2</sub>S (or a mixed gas of H<sub>2</sub>S and H<sub>2</sub>), which is toxic and corrosive. Excessive S powder was used to create an atmosphere in which the chlorides were sure to completely change to MoS<sub>2</sub> or WS<sub>2</sub>. The whole reaction system was tightly sealed and protected by a flow of argon, because traces of oxygen could cause oxidation of the products. Furthermore, the by-product S<sub>2</sub>Cl<sub>2</sub> is a toxic material with a pungent smell, and although the amount produced was quite small, NaOH solution was used to absorb the S<sub>2</sub>Cl<sub>2</sub> and convert it into innocuous materials according to Equation (6).<sup>[26]</sup>



A more detailed investigation of the reaction between chlorides and sulfur was done by choosing the reaction of MoCl<sub>5</sub> and S as a model. A series of controlled experiments were conducted at temperatures between 200 and 900 °C. Although the reaction of MoCl<sub>5</sub> and S began at about 300 °C, MoS<sub>2</sub> was formed at higher temperatures. Figure 10a shows the typical XRD patterns of the products obtained at 300, 450, 480, 515, 550, 615, and 850 °C. As shown in this figure, MoS<sub>2</sub> was not obtained until the reaction temperature was greater than 550 °C. It was found that MoS<sub>2</sub> had a rhombohedral structure at 550 °C and a hexagonal structure at 850 °C. At an intermediate temperature of about 615 °C, MoS<sub>2</sub> consisted of a mixture of rhombohedral and hexagonal phases.

From the experiments, the reaction of MoCl<sub>5</sub> and S is believed to be a stepwise sulfurization reaction.

At first, MoCl<sub>5</sub> is reduced and partially sulfurized forming the intermediate product of MoS<sub>x</sub>Cl<sub>y</sub>. Upon further reaction with sulfur atoms, chlorine atoms in the intermediate are substituted by sulfur atoms, and the pure MoS<sub>2</sub> phase is obtained. MoS<sub>x</sub>Cl<sub>y</sub> intermediate products were obtained at low reaction temperatures, providing strong evidence of this mechanism. X-ray photoelectron spectroscopy (XPS) was carried out on the intermediate samples and indicated that the products contained Mo, S, and Cl atoms. The intermediate products obtained at different temperatures had different molar ratios of Mo, S, and Cl; for example, at 515 °C, the molar ratio was about 0.35:0.42:0.24. Figure 10b and c presents the typical XPS spectra of the Mo 3d and S 2p, corresponding to the intermediate sample obtained at 515 °C. In Figure 10b, the Mo 3d<sub>5/2</sub> peak at 229.8 eV and the Mo 3d<sub>3/2</sub> peak at 233.0 eV could be attributed to Mo<sup>4+</sup> atoms.<sup>[31]</sup> In Figure 10c, the S 2p spectrum primarily showed a strong peak at about 162.9 eV, the same as that for conventional MoS<sub>2</sub>. These results agree with the mechanism detailed above. We obtained the pure MoS<sub>2</sub> phase by heating the intermediate samples to 800 °C in an argon atmosphere, with or without sulfur. This result further supported the premise of MoS<sub>x</sub>Cl<sub>y</sub> being the intermediate product of the reaction of MoCl<sub>5</sub> and S. This reaction was very fast at high temperatures: We took samples at 850 °C for different time periods, which were then examined by XRD. The results showed that MoS<sub>2</sub> had been formed after a 2 min reaction. Thus, we failed to obtain the intermediate products. More work is needed for a better understanding of the reaction mechanism.

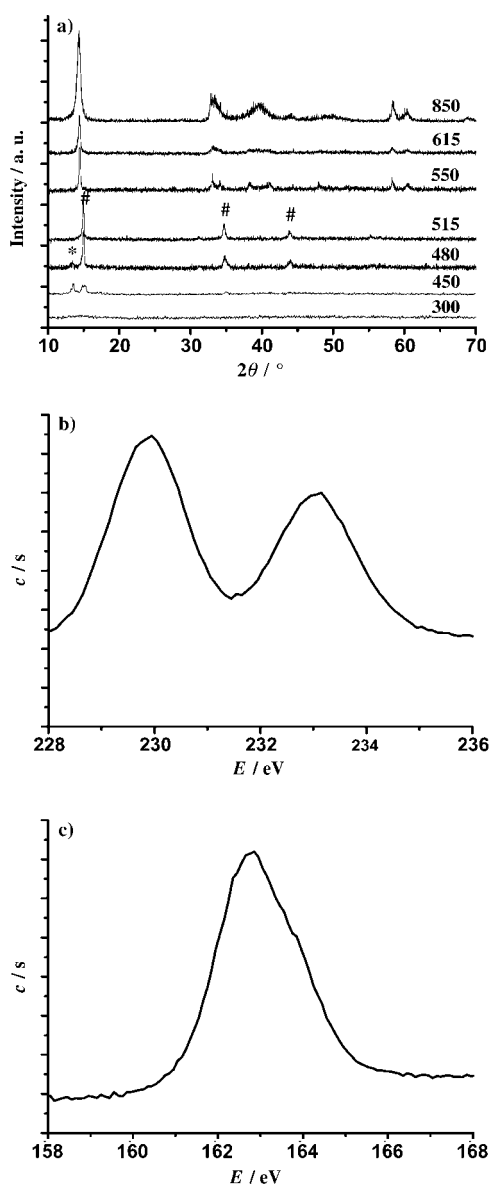


Figure 10. a) XRD patterns of the reaction products of MoCl<sub>5</sub> and S, obtained at different reaction temperatures. (Temperatures given in °C; # and \* indicate intermediate products of MoS<sub>2</sub>Cl<sub>x</sub>.) The XPS spectra of the intermediate product obtained at 515 °C: b) Mo 3d spectrum, c) S 2p spectrum.

**Formation of MoS<sub>2</sub> and WS<sub>2</sub> IF nanoparticles:** According to the literature<sup>[8,26–30]</sup> and our experimental results, it is believed that MoS<sub>2</sub> and WS<sub>2</sub> IF nanostructures are formed in vapor, and the growth is dominated by the vapor–solid (VS) mechanism. By heating the reactants directly to 850 °C, the chlorides (MoCl<sub>5</sub> or WCl<sub>6</sub>) and S quickly evaporate and simultaneously react. Similar to the reactions detailed in references [29–31], which were highly exothermic at elevated temperatures, ignition of the present reaction at high temperature led to a very rapid and sometimes explosive reaction progression. This rapid reaction might lead to a high degree of supersaturation of the vapor and hence, to fast nucleation. Thus, numerous nuclei of IF MoS<sub>2</sub>/WS<sub>2</sub> are initially formed in the vapor phase. Some nuclei grow larger relative

to others and subsequently precipitate on the substrates at 850 °C. Layered structures with relatively large radii of curvature (> 10 nm) and thin walls form and bend, resulting in quasi-spherical fullerene-like nanostructures.<sup>[32]</sup> Thus, when the initial clusters grow to the critical size, they bend and form incipient IF structures. These clusters grow, crystallize, and finally form spherical IF nanoparticles. When the dimensions of the nanostructures are below the critical size, the bending energy is excessively high, and point defects become energetically favorable. IF nanostructures with many dislocations, partially closed layers, or faceted polyhedral structures form, as has been validated by the growth of WS<sub>2</sub> IF nanoparticles from tungsten oxide nanoparticles.<sup>[19]</sup> Although in our approach, the reaction reached completion very quickly at high temperatures, the annealing treatment lasted for 1 h. During this process, defects and amorphous products in the IF nanoparticles grew further, resulting in well-crystallized IF nanostructures.

Other nuclei formed initially might be transported downstream by the argon flow and deposited in low-temperature regions. Because temperature plays an important role in controlling the shape and crystallization of the products, the clusters deposited at different temperatures must have different thermodynamic and kinetic growth behavior. Thus, nanoflowers and nanotubes were obtained separately at about 650 and 750 °C.

**Surface area measurement and field-emission effect:** The surface area of as-synthesized MoS<sub>2</sub> IF nanoparticles, determined by Brunauer–Emmett–Teller (BET) gas adsorption isothermals, was found to be about 33.4 m<sup>2</sup>g<sup>-1</sup>, much larger than that of MoS<sub>2</sub> nanoflowers, usual MoS<sub>2</sub> crystals, and some MoS<sub>2</sub> nanotube samples.<sup>[33–34]</sup> With this large surface area, as-synthesized IF MoS<sub>2</sub> samples were expected to have excellent performance in areas such as catalysis, hydrogen storage, and as catalysts carriers. Detailed measurements are provided in the Supporting Information.

Stimulated by the field-emission effect of low-dimensional nanomaterials,<sup>[35–40]</sup> and the flowerlike structure with numerous nanosized free-edges, we investigated the field-emission effect of the as-synthesized WS<sub>2</sub> nanoflowers. They appeared to be good field emitters, displaying current densities of 0.01 and 0.6 mA cm<sup>-2</sup> at macroscopic fields of about 6.1 and 8.3 V μm<sup>-1</sup>, respectively. The Fowler–Nordheim (FN) plots, corresponding to different separations, showed a similar linear relationship and revealed that electron emission from WS<sub>2</sub> nanoflowers followed the FN theory. Details of these measurements can be found in the Supporting Information.

## Conclusion

We have prepared large-scale MoS<sub>2</sub> and WS<sub>2</sub> IF nanostructures and elegant three-dimensional nanoflowers by the reaction of chlorides and S in a designed atmospheric pressure chemical vapor deposition route. The reaction mechanism was proposed on the basis of the experimental facts. The surface area of MoS<sub>2</sub> IF nanoparticles and the field-emission

effect of as-synthesized WS<sub>2</sub> nanoflowers were reported. This synthetic strategy provides an alternative method for the large-scale synthesis of MoS<sub>2</sub> and WS<sub>2</sub> IF nanostructures, and might offer an opportunity for the extensive investigation of their vast number of applications.

## Experimental Section

**Materials:** The molybdenum pentachloride (MoCl<sub>5</sub>), tungsten hexachloride (WCl<sub>6</sub>), and all chemicals used in this work were analytical grade reagents. Single crystal (100) silicon wafers were used as substrates.

**Synthesis:** The typical synthesis process was carried out in a conventional tube furnace at about 850 °C, with an argon flow-rate of about 20 sccm (standard cubic centimeter per minute). The MoCl<sub>5</sub>/WCl<sub>6</sub> (about 2 mmol) was loaded into a quartz boat and placed in the middle of the quartz tube. Excessive sulfur (about 20 mmol) was loaded into another quartz boat and placed 5 cm away from the chlorides in the upstream end of the tube. Silicon substrates (5 × 5 mm<sup>2</sup>) were arranged neatly in a quartz boat, which was located 5 cm away from the chlorides in the downstream end of the quartz tube. When the furnace temperature became stable at 850 °C, the reactants were quickly pushed into the hot zone of the furnace. After the sample had been annealed at 850 °C for 1 h, it was cooled in the furnace to room temperature in an argon atmosphere. The products deposited at different temperature regions were carefully collected for characterization. In general, fullerene-like nanoparticles, nanotubes, and nanoflowers were deposited at about 850, 750, and 650 °C, respectively. The total yield of MoS<sub>2</sub>/WS<sub>2</sub> was calculated to be about 95% on the basis of Mo/W. With optimized reaction factors we could obtain more than 90% single-morphology product in one port.

**Characterization:** Powder X-ray diffraction was performed on a Bruker D8-Advance X-ray diffractometer with Cu<sub>Kα</sub> radiation ( $\lambda = 1.54178 \text{ \AA}$ ). The  $2\theta$  range used in the measurement was from 10° to 70° in steps of 0.02° with a count time of 1 s. The size and morphology of as-synthesized samples were determined by using a Hitachi model H-800 transmission electron microscope (tungsten filament) at an accelerating voltage of 200 kV. The structure and composition of the products were characterized by a JEOL-2010F high-resolution transmission electron microscope and energy-dispersive X-ray spectroscopy. SEM images were carried out on a JSM-6301F scanning electron microscope. Raman spectra were taken on a RM 2000 microscope and confocal Raman spectrometer (Renishaw PLC., England), which included a 632.8 nm laser beam and a CCD detector with 4 cm<sup>-1</sup> resolution. X-ray photoelectron spectroscopy was carried out using a PHI-5300 ESCA.

## Acknowledgements

This work was supported by NSFC (20025102, 50372030, 20151001), the Foundation for the Author of National Excellent Doctoral Dissertation of P. R. China, and the State Key Project of Fundamental Research for nanomaterials and nanostructures (2003CB716901).

- [1] H. W. Kroto, J. R. Heath, S. C. O'Brien, R. F. Crul, R. E. Smalley, *Nature* **1985**, *318*, 162–163.
- [2] S. Iijima, *Nature* **1991**, *354*, 56–58.
- [3] W. Kraetschmer, L. D. Lamb, K. Fostiropoulos, D. R. Huffman, *Nature* **1990**, *347*, 354–358.
- [4] a) R. Tenne, L. Margulis, M. Genut, G. Hodes, *Nature* **1992**, *360*, 444–446; b) L. Margulis, G. Salitra, R. Tenne, M. Talianker, *Nature* **1993**, *365*, 113–114; c) Y. Feldman, E. Wasserman, D. J. Srolovitz, R. Tenne, *Science* **1995**, *267*, 222–225.
- [5] N. G. Chopra, R. J. Luyren, K. Cherry, V. H. Crespi, M. L. Cohen, S. G. Louis, A. Zettl, *Science* **1995**, *269*, 966–967.
- [6] Y.-D. Li, J. W. Wang, Z. X. Deng, Y. Y. Wu, X. M. Sun, D. P. Yu, P. D. Yang, *J. Am. Chem. Soc.* **2001**, *123*, 9904–9905.
- [7] a) M. E. Spahr, P. Betterli, R. Nesper, M. Müller, F. Krumeich, H. U. Nissen, *Angew. Chem.* **1998**, *110*, 1339–1342; *Angew. Chem. Int. Ed.* **1998**, *37*, 1263–1265; b) F. Krumeich, H. J. Muhr, M. Niederberger, F. Bieri, B. Schnyder, R. Nesper, *J. Am. Chem. Soc.* **1999**, *121*, 8324–8331; c) M. Niederberger, H. J. Muhr, F. Krumeich, F. Bieri, D. Gunther, R. Nesper, *Chem. Mater.* **2000**, *12*, 1995–2000.
- [8] a) M. Nath, C. N. R. Rao, *J. Am. Chem. Soc.* **2001**, *123*, 4841–4842; b) C. Schuffenhauer, R. Popovitz-Biro, R. Tenne, *J. Mater. Chem.* **2002**, *12*, 1587–1591; c) Y. Q. Zhu, W. K. Hsu, H. W. Kroto, D. R. M. Walton, *Chem. Commun.* **2001**, 2184–2185.
- [9] a) M. Brorson, T. W. Hansen, C. J. H. Jacobsen, *J. Am. Chem. Soc.* **2002**, *124*, 11582–11583; b) K. S. Coleman, J. Sloan, N. A. Hanson, G. Brown, G. P. Clancy, M. Terrones, H. Terrones, M. L. H. Green, *J. Am. Chem. Soc.* **2002**, *124*, 11580–11581.
- [10] a) M. Nath, C. N. R. Rao, *Angew. Chem.* **2002**, *114*, 3601–3604; *Angew. Chem. Int. Ed.* **2002**, *41*, 3451–3454; b) J. Chen, S. L. Li, Z. L. Tao, Y. T. Shen, C. X. Cui, *J. Am. Chem. Soc.* **2003**, *125*, 5284–5285.
- [11] S. Y. Hong, R. Popovitz-Biro, Y. Prior, R. Tenne, *J. Am. Chem. Soc.* **2003**, *125*, 10470–10474.
- [12] a) M. Chhowalla, G. A. J. Amaratunga, *Nature* **2000**, *407*, 164–167; b) L. Rapoport, Y. Bilik, Y. Feldman, M. Homyonfer, S. R. Cohen, R. Tenne, *Nature* **1997**, *387*, 791–793; c) Y. Golan, C. Drummond, M. Homyonfer, Y. Feldman, R. Tenne, J. Israelachvili, *Adv. Mater.* **1999**, *11*, 934–937.
- [13] N. Imanishi, K. Kanamura, Z. Takehara, *J. Electrochem. Soc.* **1992**, *139*, 2082–2087.
- [14] J. Chen, S. L. Li, Q. Xu, K. Tanaka, *Chem. Commun.* **2002**, 1722–1723.
- [15] J. Chen, N. Kuriyama, H. Yuan, H. T. Takeshita, T. Sakai, *J. Am. Chem. Soc.* **2001**, *123*, 11813–11814.
- [16] a) A. Zak, Y. Feldman, V. Lyakhovitskaya, G. Leitus, R. Popovitz-Biro, E. Wachtel, H. Cohen, S. Reich, R. Tenne, *J. Am. Chem. Soc.* **2002**, *124*, 4747–4758; b) M. Remskar, Z. Skraba, P. Stadelmann, F. Levy, *Adv. Mater.* **2000**, *12*, 814–818; c) M. Homyonfer, B. Alperson, Y. Rosenberg, L. Sapir, S. R. Cohen, G. Hodes, R. Tenne, *J. Am. Chem. Soc.* **1997**, *119*, 2693–2698.
- [17] A. Rothschild, S. R. Cohen, R. Tenne, *Appl. Phys. Lett.* **1999**, *75*, 4025–4027.
- [18] a) R. Tenne, *Adv. Mater.* **1995**, *7*, 965–995; b) R. Tenne, *Chem. Eur. J.* **2002**, *8*, 5297–5304; c) R. Tenne, M. Homyonfer, Y. Feldman, *Chem. Mater.* **1998**, *10*, 3225–3238; d) C. N. R. Rao, M. Nath, *Dalton Trans.* **2003**, *1*, 1–24.
- [19] a) Y. Feldman, G. L. Frey, M. Homyonfer, V. Lyakhovitskaya, L. Margulis, H. Cohen, G. Hodes, J. L. Hutchison, R. Tenne, *J. Am. Chem. Soc.* **1996**, *118*, 5362–5367; b) A. Zak, Y. Feldman, V. Alperovich, R. Rosentsveig, R. Tenne, *J. Am. Chem. Soc.* **2000**, *122*, 11108–11116; c) A. Rothschild, J. Sloan, R. Tenne, *J. Am. Chem. Soc.* **2000**, *122*, 5169–5179.
- [20] C. M. Zelenski, P. K. Dorhout, *J. Am. Chem. Soc.* **1998**, *120*, 734–742.
- [21] M. Nath, A. Govindaraj, C. N. R. Rao, *Adv. Mater.* **2001**, *13*, 283–286.
- [22] a) W. K. Hsu, B. H. Chang, Y. Q. Zhu, W. Q. Han, H. Terrones, M. Terrones, N. Grobert, A. K. Cheetham, H. W. Kroto, D. R. M. Walton, *J. Am. Chem. Soc.* **2000**, *122*, 10155–10158; b) Y. Q. Zhu, W. K. Hsu, N. Grobert, B. H. Chang, M. Terrones, H. Terrones, H. W. Kroto, D. R. M. Walton, *Chem. Mater.* **2000**, *12*, 1190–1194.
- [23] M. Remskar, A. Mrzel, Z. Skraba, A. Jesih, M. Ceh, J. Demsar, P. Stadelmann, F. Levy, D. Milhailovic, *Science* **2001**, *292*, 479–481.
- [24] Y.-D. Li, X. L. Li, R. R. He, J. Zhu, Z. X. Deng, *J. Am. Chem. Soc.* **2002**, *124*, 1411–1416.
- [25] Y. Feldman, A. Zak, R. Popovitz-Biro, R. Tenne, *Solid State Sci.* **2000**, *2*, 663–672.
- [26] a) X. L. Li, Y.-D. Li, *Chem. Eur. J.* **2003**, *9*, 2726–2731; b) J. P. Ge, Y.-D. Li, *Chem. Commun.* **2003**, *19*, 2498–2499; c) J. P. Ge, Y.-D. Li, *Adv. Funct. Mater.* **2004**, *14*, 157–162.
- [27] a) G. L. Frey, R. Tenne, M. J. Matthews, M. S. Dresselhaus, G. Dresselhaus, *Phys. Rev. B* **1999**, *60*, 2883–2892; b) A. M. Stacy, D. T. Hodul, *J. Phys. Chem. Solids* **1985**, *46*, 405–409; c) T. J. Wieting, J. L. Verble, *Phys. Rev. B* **1971**, *3*, 4286–4292.

- [28] a) I. Endler, A. Leonhardt, U. König, H. van den Berg, W. Pitschke, V. Sottke, *Surf. Coat. Technol.* **1999**, *120*, 482–488; b) W. Y. Lee, T. M. Besmann, M. W. Stott, *J. Mater. Res.* **1994**, *9*, 1474–1482; c) E. Stoffels, W. W. Stoffels, G. Ceccone, R. Hasnaoui, H. Keune, G. Wahl, F. Rossi, *J. Appl. Phys.* **1999**, *86*, 3442–3451.
- [29] V. W. Biltz, P. Ehrlich, K. Meisel, *Z. Anorg. Allg. Chem.* **1937**, 234, 97.
- [30] P. R. Bonneau, R. F. Jarvis, Jr., R. B. Kaner, *Nature* **1991**, *349*, 510–512.
- [31] a) D. Briggs, M. P. Seah, *Practical Surface Analysis Vol. 1*, 2nd ed., Wiley, New York, **1990**; b) C. D. Wagner, W. M. Riggs, L. E. Davis, J. F. Moulder, G. E. Muilenberg, *Handbook of X-Ray Photoelectron Spectroscopy*, Perkin-Elmer, Eden Prairie MN, **1979**; c) R. B. Quincy, M. Houalla, A. Proctor, D. M. Hercules, *J. Phys. Chem.* **1990**, *94*, 1520–1526.
- [32] D. J. Srolovitz, S. A. Safran, M. Homyonfer, R. Tenne, *Phys. Rev. Lett.* **1995**, *74*, 1779–1782.
- [33] a) K. E. Dungey, M. D. Curtis, J. E. Penner-Hahn, *J. Catal.* **1998**, *175*, 129–134; b) Y. Iwata, K. Sato, T. Yoneda, Y. Miiki, Y. Sugimoto, A. Nishijima, H. Shimada, *Catal. Today* **1998**, *45*, 353–359; c) X. Bokhimi, J. A. Toledo, J. Navarrete, X. C. Sun, M. Portilla, *Int. J. Hydrogen Energy* **2001**, *26*, 1271–1277.
- [34] a) J. Chen, S. L. Li, Z. L. Tao, *J. Alloys Compd.* **2003**, *356*, 413–417; b) J. Chen, S. L. Li, F. Gao, Q. Xu, K. Tanaka, *Sci. China Ser. B* **2003**, *46*, 191–195.
- [35] a) S. S. Fan, M. G. Chapline, N. R. Franklin, T. W. Tombler, A. M. Cassell, H. J. Dai, *Science* **1999**, *283*, 512–514; b) C. H. Poa, S. R. P. Silva, R. C. P. Watts, W. K. Hsu, H. W. Kroto, D. R. M. Walton, *Appl. Phys. Lett.* **2002**, *80*, 3189–3141.
- [36] Z. S. Wu, S. Z. Deng, N. S. Xu, J. Chen, J. Zhou, J. Chen, *Appl. Phys. Lett.* **2002**, *80*, 3829–3831.
- [37] Y. Lee, C. Choi, Y. Jang, E. Kim, B. Ju, N. Min, J. Ahn, *Appl. Phys. Lett.* **2002**, *81*, 745–747.
- [38] Y. B. Li, Y. Bando, D. Golberg, K. Kurashima, *Appl. Phys. Lett.* **2002**, *81*, 5048–5050.
- [39] Y. W. Zhu, H. Z. Zhang, X. C. Sun, S. Q. Feng, J. Xu, Q. Zhao, B. Xiang, R. M. Wang, D. P. Yu, *Appl. Phys. Lett.* **2003**, *83*, 144–146.
- [40] Y. B. Li, Y. Bando, D. Golberg, *Appl. Phys. Lett.* **2003**, *82*, 1962–1964.

Received: May 8, 2004

Published online: October 29, 2004